ACS Catalysis

Research Article

pubs.acs.org/acscatalysis

Synergetic Role of Photogenerated Electrons and Holes in the Oxidation of CO to CO_2 on Reduced TiO_2(110): A First-Principles Study

Kyoung E. Kweon,[†] Dhivya Manogaran,[‡] and Gyeong S. Hwang*[,†]

[†]Department of Chemical Engineering and [‡]Department of Chemistry and Biochemistry, University of Texas at Austin, Austin, Texas 78712, United States

Supporting Information

ABSTRACT: We present the role of photogenerated charge carriers in the oxidation of CO by O_2 on reduced, rutile TiO_2(110) based on first-principles DFT calculations. Our calculations show that hole-trapped O_2 at the O vacancy site adopts a tilted open ring configuration, while an additional electron preferentially localizes at the CO-bound Ti site. The electron−hole separated configuration likely converts to the O−O−C−O complex with a small barrier of around 0.1 eV. From the neutral intermediate state, CO_2 is predicted to desorb off the surface with a barrier less than 0.2 eV if another hole is available. For comparison, we also look at both thermally activated and hole-mediated CO oxidation processes, but the predicted overall barriers of around 0.9 and 0.5 eV, respectively, appear to be high for facile CO oxidation at low temperatures. Our findings clearly highlight that excess electrons and holes can synergetically contribute to CO photooxidation, which is consistent with a recent experimental study by Petrik and Kimmel that provides evidence for involvement of multiple nonthermal reaction steps.

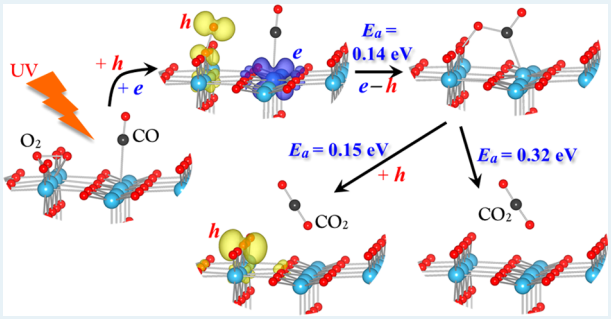

KEYWORDS: *CO photooxidation, rutile TiO_2(110), synergetic role of electrons and holes, nonthermal catalytic reaction, density functional theory calculation*

I. INTRODUCTION

TiO_2 has been widely used as a photocatalyst because of its high catalytic efficiency, high chemical stability, and low cost.[1−5] Successful utilization of its photocatalysis is now seen in various industrial applications such as self-cleaning windows, antimicrobial coating, and water and air purification.[1−7] In principle, TiO_2 photocatalysis involves electron−hole pair creation by UV absorption followed by the reaction of the photogenerated charge carriers with chemical species at the surface. However, the detailed underlying mechanisms often remain controversial.

Several experimental and theoretical studies have been undertaken to explore mechanisms underlying the reaction of CO and O_2 on a reduced rutile TiO_2(110) surface under UV irradiation; the CO photooxidation has received considerable attention due to its fundamental significance as a prototype photocatalytic system. First-principles calculations[8,9] have predicted that O_2 chemisorbed at an oxygen vacancy site may react with CO adsorbed on an adjacent Ti site to produce CO_2 via an intermediate complex (O−O−C−O or O−O−Ti—C−O), which is well supported by the off-normal desorption behavior of CO_2 that has been experimentally observed.[10] The predicted energy barrier for the thermally activated oxidation of CO is around 0.4−0.8 eV, which appears to be too high for facile CO oxidation at low temperatures (<105 K) as reported under UV irradiation.[10−15] This suggests the importance of nonthermal reactions mediated by photogenerated charge carriers. From their experimental study, Zhang and Yates concluded that the photooxidation of CO on TiO_2(110) would be an electron-mediated process, as it was found to be suppressed by upward band bending in the presence of electron-acceptor molecules.[13] In addition, a recent theoretical study by Ji et al.[9] suggested the possible contribution of holes to reducing the activation barrier for CO oxidation. Very recently, Petrik and Kimmel brought into notice the possibility of two or more nonthermal reaction steps being involved in CO photooxidation on reduced, rutile Ti(110).[15]

In this work, we examine how photogenerated electrons and holes can contribute to the oxidation of CO by O_2 on a partially reduced rutile TiO_2(110) surface. Our calculations are performed within the framework of spin-polarized density functional theory (DFT) with Hubbard U corrections, which has been shown to well characterize charge localization, while standard DFT erroneously favors charge delocalization due to its inherent self-interaction error; for comparison, standard and hybrid DFT calculations were also performed for selected cases.

Received: July 22, 2014
Revised: September 19, 2014
Published: October 1, 2014

   dx.doi.org/10.1021/cs5010568 | ACS Catal. 2014, 4, 4051−4056

First, we revisit the reaction pathways and energetics of thermally-activated CO oxidation with comparisons to previous theoretical studies. Then, we present hole-mediated CO oxidation with careful analysis of hole localization and the reaction mechanisms involved. Finally, we investigate the synergetic catalytic role played by excess electrons and holes in facilitating CO oxidation.

II. COMPUTATIONAL METHODS

All calculations reported herein were performed using DFT with Hubbard U correction (DFT+U)[16] within the generalized gradient approximation (GGA-PBE),[17] as implemented in the Vienna Ab-initio Simulation Package (VASP 5.2.2).[18] For comparison, we also performed standard GGA and hybrid DFT calculations to evaluate the relative energies of the initial, intermediate, and final states of the reactions examined, as summarized in Table S1 (Supporting Information); even though there are some noticeable variations in the reaction energetics, the overall conclusions of this article remain largely unaffected by the choice of the calculation method. Spin polarization was also considered to describe properly unpaired electrons. We employed the projected augmented wave method[19] with a plane-wave basis set (which was truncated at a cutoff energy of E_{cut} = 450 eV). The rutile TiO_2(110) surface was modeled using a periodic six-layer slab with a (4 × 2) surface supercell and a vacuum gap of 10 Å in the z direction, as depicted in Figure 1; the slab thickness was chosen through a careful examination of its dependence of the reaction energetics (see Supporting Information Table S1). For Brillouin zone integration, one k point (at Γ) and a Γ-centered (2 × 2 × 1) Monkhorst–Pack mesh were used in geometry optimization and electronic structure refinement, respectively; the convergence with respect to E_{cut} and k point sampling was carefully checked. All atoms in the slab were allowed to fully relax until the residual forces on all the constituent atoms become smaller than 0.02 eV/Å. The Hubbard-U correction was applied to both Ti 3d and O 2p electrons with fixed values of $U_{Ti}(d)$ = 3.3 eV and $U_O(p)$ = 4.0 eV (which have been used by other theoretical studies[20−24] and shown to well reproduce experimental observations such as localized Ti d states on a partially reduced rutile TiO_2(110) surface[25,26]); $U_O(p)$ = 4.0 eV was also applied to the 2p electrons of the O atoms in O_2 and CO. We also considered $U_{Ti}(d)$ = 4.2 eV and $U_O(p)$ = 5.0 eV as employed by others,[27,28] but the results show no significant difference from those reported herein (see Supporting Information Table S1).

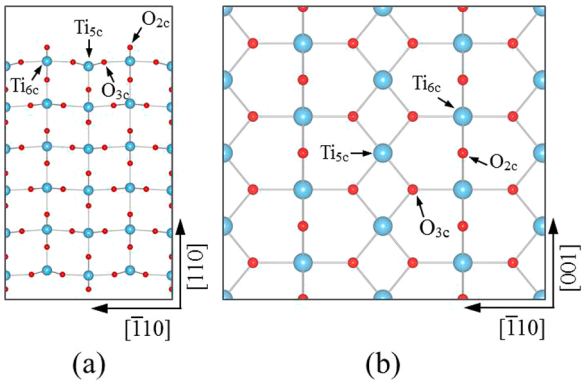

Figure 1. (a) Side and (b) top view of the periodic six-layer slab with a (4 × 2) surface supercell that is used to model the rutile TiO_2(110) surface. 5-fold coordinated Ti_{5c}, 6-fold coordinated Ti_{6c}, 2-fold coordinated bridging O_{2c}, and 3-fold coordinated in-plane O_{3c} atoms are indicated. Light blue and red balls represent Ti and O atoms, respectively.

For the charged system with an excess hole (or electron), one electron was removed from (or added to) the neutral system, and the charge neutrality was ensured within the supercell by adding a compensating homogeneous background charge; here, the coulomb energy between the excess charge and the background charge was ignored due to the large dielectric constant of rutile TiO_2.[29] A localized hole (or electron) state was created by initially applying a small perturbation around the O (or Ti) atom (where the excess charge is expected to be localized) to break the lattice symmetry prior to structural relaxation;[30] here, only the lowest energy structure is reported among several different sites examined for charge localization. Reaction pathways and barriers were determined using the climbing-image nudged elastic band (CI-NEB) method[31] with 6−8 intermediate images for each elementary step, and the transition states were further refined using the dimer method.[32]

III. RESULTS AND DISCUSSION

For comparison, first we revisited the pathways for CO_2 formation from coadsorbed CO and O_2 on a partially reduced TiO_2 (110) surface (which was created by removing one bridging O atom). The rutile (110) surface comprises of two types of Ti atoms (i.e., 5-fold coordinated Ti_{5c} and 6-fold coordinated Ti_{6c}) and two types of O atoms (i.e., 2-fold coordinated bridging O_{2c} and 3-fold coordinated in-plane O_{3c}) (see Figure 1). As illustrated in Figure 2(a), in the coadsorption state **A**, O_2 prefers to adsorb horizontally at the oxygen vacancy (V_O) site while CO exists vertically at an adjacent Ti_{5c} site.[8,9] A CO molecule is known to interact with the TiO_2(110) surface mainly through its 5σ state,[33−36] as seen from the density of states (DOS) analysis in Figure 3 that displays significant overlap of the CO 5σ and Ti d states. In addition, from the DOS analysis, we find the O_2 π^* states to be filled exhibiting the peroxo-like character, as also demonstrated by previous calculations;[8,9,37] note also that the O−O bond distance of 1.46 Å is close to the 1.48 Å for O_2^{2-} in HOOH. Compared to the separately adsorbed case (see Figure S1 in the Supporting Information), in the coadsorbed state, the projected DOS displays a slight 5σ splitting as shown in Figure 3, which could be attributed to the nonbonded molecular interaction between CO and O_2. However, such interaction turns out to have insignificant influence on CO binding to the surface; that is, the predicted CO adsorption energy of 0.37 eV remains nearly identical in changing the binding Ti site with respect to O_2. It is also worthwhile to point out that the CO binding energy of 0.38 eV on the stoichiometric surface is similar to the reduced surface case, suggesting that an adsorbed O_2 molecule could passivate an O vacancy on reduced TiO_2(110).[8,37]

Figure 2 shows two possible CO oxidation pathways each of which involves an intermediate state. First, the adsorbed O_2 attains a tilted configuration and leans either toward adjacent Ti_{5c} forming **B1** or toward the C atom of adsorbed CO forming **B2**; the intermediate states have been also identified by earlier studies.[8,9] The activation energies (E_a) involved in the formation of **B1**/**B2** are predicted to be E_a = 0.78/0.87 eV, in good agreement with other DFT-GGA calculations.[9] In the intermediate states, O_2 is still found to have a peroxo-like

dx.doi.org/10.1021/cs5010568 | ACS Catal. 2014, 4, 4051−4056

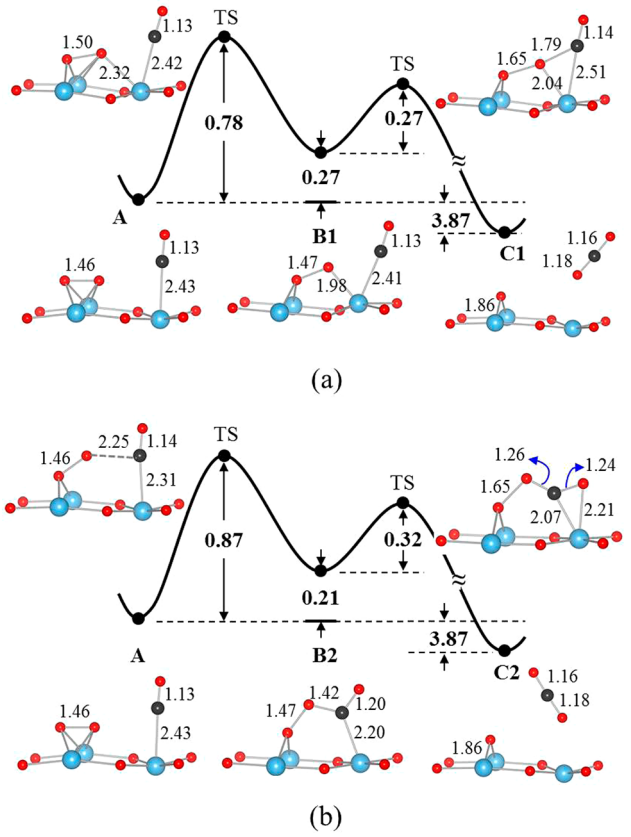

Figure 2. Predicted potential energy variations (in eV) for CO production from coadsorbed CO and O_2 through two different reaction pathways (a) **A-B1-C1** and (b) **A-B2-C2**, together with corresponding initial, intermediate, final, and transition state configurations; selected bond distances are also shown in Å. Light blue, red, and dark gray balls represent Ti, O, and C atoms, respectively.

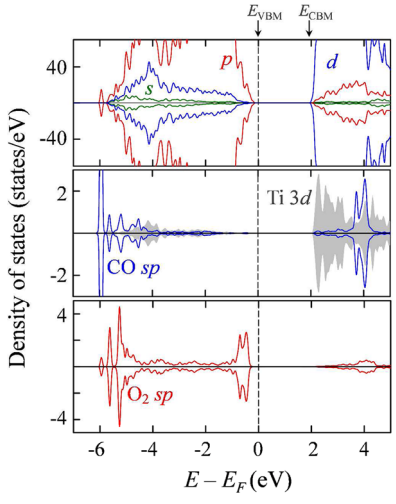

Figure 3. Density of states (DOS) for the partially reduced TiO_2(110) system with coadsorbed CO and O_2 (see state **A** in Figure 2); (*top*) the *s*, *p*, and *d* states of all C, O, and Ti atoms in the TiO_2(110) slab with CO and O_2, (*middle*) the 3*d* states of CO-bound Ti_{5c} and the CO *s* and *p* states, and (*bottom*) the *s* and *p* states of O_2 adsorbed at the O vacancy site, as indicated. The vertical dashed line indicates the position of the Fermi level (E_F) which is set equal to zero, and the valence band maximum (E_{VBM}) and the conduction band minimum (E_{CBM}) positions are also indicated.

character with a bond distance of 1.47 Å, while the Ti−C bond distance in **B2** is reduced to 2.20 Å compared to 2.41 Å in **B1**. The relatively enhanced Ti−C interaction in **B2** is attributed to the increased CO 5σ and Ti *d* interaction, as seen in Figure S2 in the Supporting Information. We also checked the possible interconversion between **B1** and **B2**, but the predicted sizable barrier of 0.55 eV suggests that they can form two probable distinct intermediate states.

Next, from **B1**, CO_2 desorbs off by cleaving the O−O bond, which requires overcoming a barrier of 0.27 eV (see **C1**). From **B2**, for CO_2 desorption, the transition state is predicted to involve a significant interaction of O (from CO) and Ti_{5c} while weakening the O−O bond interaction. Then, the O−O bond is broken reorienting the CO_2 molecule, facilitating the desorption by overcoming a barrier of 0.32 eV (see **C2**). Note also that the orientation of CO_2 in both **C1** and **C2** is perpendicular to the bridging O rows, which is consistent with previous experimental observations;[10] in addition, it would be worth pointing out that CO_2 may physisorb such that the TiO_2 surface could also be populated with CO_2 at very low temperatures (<140 K).[38]

Next, we examined how an excess hole (h) affects the CO oxidation. The h added to state **A** is found to preferentially localize on O_2. This is not surprising given that the O_2 *sp* states in **A** are located at the top of the valence band, i.e., they are readily available to accept a hole, as demonstrated by the DOS analysis (see Figure 3); we also considered a hole trapped at a bridging O atom, but it turns out to be energetically less favorable than the hole trapping at adsorbed O_2.

Recent experiments also provide evidence that an excess hole would prefer to occupy an O_2 site rather than a lattice O site.[14] The hole trapping results into a tilted open ring configuration $\mathbf{A_H}$, in which the O_2 has a superoxo (O_2^-) like character with an O−O bond distance of 1.35 Å (see Figure 4).

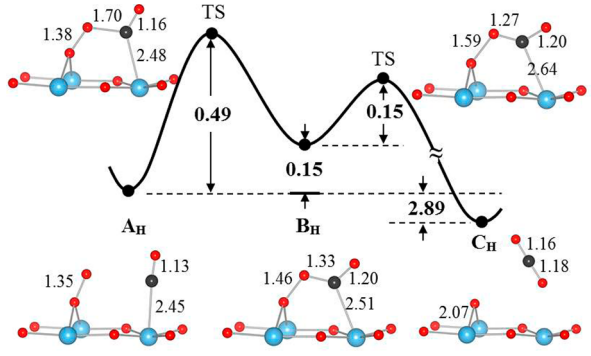

Figure 4. Predicted potential energy variations (in eV) for hole-mediated CO production from coadsorbed CO and O_2, together with corresponding initial, intermediate, final, and transition state configurations; selected bond distances are also shown in Å. Light blue, red, and dark gray balls represent Ti, O, and C atoms, respectively.

In $\mathbf{A_H}$, the terminal oxygen in O_2 (referred to as O_I, hereafter) is predicted to mainly possess the excess h, as illustrated by the projected DOS on O_I and O_{II} in Figure 5(a), wherein the unoccupied O_I *sp* states appear to lie within the conduction band. This may suggest that if an additional e is present along with the h in $\mathbf{A_H}$, it could favorably occupy the Ti site instead of the hole-trapped O_2 (which inspires us to look at

dx.doi.org/10.1021/cs5010568 | ACS Catal. 2014, 4, 4051−4056

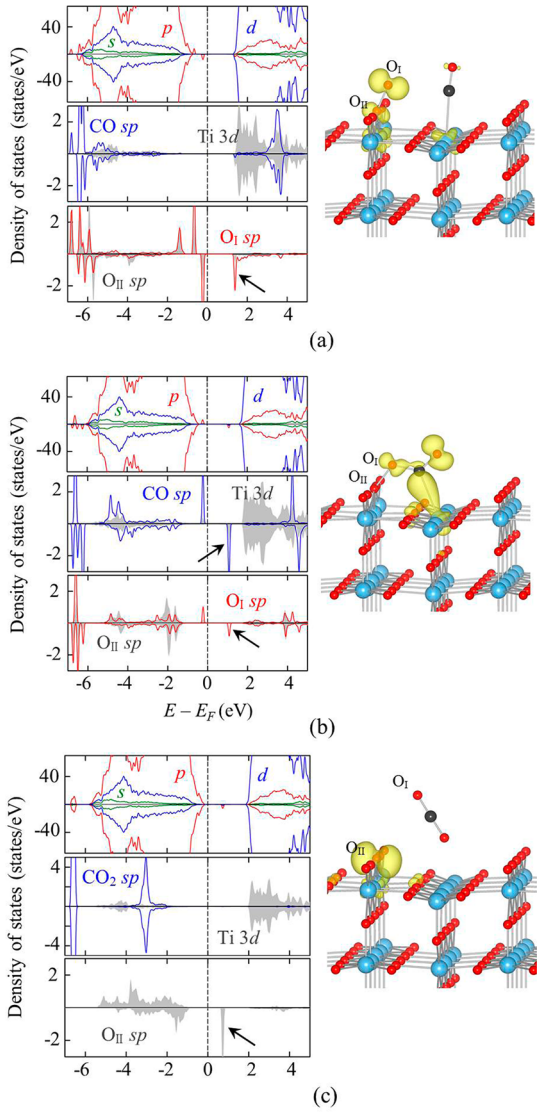

Figure 5. Density of states (DOS) for the (a) initial, (b) intermediate, and (c) final states of hole-mediated CO_2 production from coadsorbed CO and O_2; each corresponding atomic configuration is shown on the right. In each case, the top, middle, and bottom panels respectively show the *s*, *p*, and *d* states of all C, O, and Ti atoms in the TiO_2(110) slab with CO and O_2, the 3*d* states of CO-bound Ti_{5c} and the CO *s* and *p* states, and the *s* and *p* states of O_2 (or O) at the O vacancy site, as indicated. In the DOS plots, the hole states on O_2 are indicated by the arrows, and each vertical dashed line indicates the position of the Fermi level (E_F) which is set equal to zero. In each structure illustration, the yellow isosurface represents the hole states as indicated in the corresponding DOS plots; the isosurface value is set to 0.04 e/Å^3, and light blue, red, and dark gray balls represent Ti, O, and C atoms, respectively.

the configuration consisting of separated *e* and *h* at distinct sites, as discussed later).

Figure 4 shows a CO oxidation pathway identified in the presence of an *h*. Starting from $\mathbf{A_H}$, O_I in the open ring configuration interacts with the C (in CO) and forms an O_{II}−O_I—C−O complex ($\mathbf{B_H}$), which requires overcoming an activation energy of 0.49 eV. We also considered another possible intermediate, wherein, an O_{II}−O_I−Ti complex is formed (like **B1**), but the formation of such an intermediate turns out to be unlikely due to the repulsive interaction between the cationic Ti and hole-trapped O_I atoms. A similar hole-mediated pathway has been also suggested by Ji et al.,[9] but their DFT-GGA calculations with spin restriction gave a considerably lower barrier (~0.08 eV); we speculate that conventional DFT may not describe charge localization properly,[39,40] which may cause the difference from our DFT +U calculations.[21,22]

In $\mathbf{B_H}$, the *h* tends to largely delocalize over the O_{II}−O_I—C−O complex, as demonstrated by the band-decomposed charge density shown in Figure 5(b). It is apparent that the CO and TiO_2 surface interaction is weakened with an elongated Ti−C bond distance of 2.51 Å, which is also evidenced by a significantly decreased Ti *d* − CO 5 σ overlap [see Figure 5(b)] when compared to the neutral case **B2** [Figure S2(b)]. The weakened Ti−C interaction facilitates CO_2 desorption with a substantially lower activation barrier (= 0.15 eV) than the corresponding neutral case (= 0.32 eV). Once the CO_2 desorption ($\mathbf{C_H}$) takes place, the *h* that is left behind occupies the bridging O site (O_{II}), as shown in Figure 5(c). Our calculations clearly show that the presence of excess *h* significantly reduces the activation energy barrier of CO oxidation. However, the predicted value of 0.49 eV for the first step [$\mathbf{A_H}$-$\mathbf{B_H}$] appears to be still high for facile CO oxidation at low temperatures.[10−15] It would be also worth pointing out the possibility of hole-assisted O_2 desorption if two or more O_2 molecules adsorb at an V_O site, as demonstrated by previous experimental and theoretical studies.[8,10,14] However, in the case of low O_2 coverage (i.e., an O_2 molecule adsorbs at the V_O site, as considered in this work), hole-mediated O_2 desorption has been found to be less likely than CO oxidation because the hole-trapped O_2^- species can be still strongly bound to the V_O site.[14]

Finally, we further explored how the presence of an *e* in addition to the *h* contributes to altering the kinetics of CO oxidation. Here, the triplet spin state was used to obtain separate *e* and *h* configuration, while the system remains neutral; that is, initially the electron and hole states are created through local lattice distortions around the selected Ti and O atoms, respectively, prior to the structural relaxation under the spin constraint. As depicted in Figure 6, given that the *h* is trapped by O_2 (as in $\mathbf{A_H}$), the additional *e* tends to localize on the Ti_{5c} bonded to CO; as discussed earlier, the Ti *d* states are more prone to accept the additional *e* than the hole-trapped O_2 *sp* states. On the other hand, note that on the stoichiometric surface an excess *h* tends to localize on a bridging O site, inducing a unoccupied state within the gap [see Figure S3(a)]; hence, an additional *e* is expected to neutralize the *h* at bridging O site rather than occupying a Ti_{5c} site.

In the configuration with separated *e* and *h* ($\mathbf{A_{E\text{-}H}}$), the Ti−C bond distance is significantly reduced to 2.33 Å, suggesting an enhanced CO binding to the surface. The enhanced Ti−C interaction can be evidenced by the DOS (left) and band-decomposed charge density (right) plots in Figure 6 which clearly display the Ti d_{yz} and CO π interaction. This suggests that the localized *e* on Ti now enables Ti *d*-CO $2\pi^*$ back bonding; such electron back-donation is commonly seen on an electron-rich surface.[41,42] On the other hand, we would also like to mention here that in the absence of CO we found that the *e* preferentially localizes on a subsurface Ti site [see Figure S3(b)].

The *e*-*h* separated configuration $\mathbf{A_{E\text{-}H}}$ in the triplet state is predicted to be 0.85 eV higher in energy than the configuration **A** (with no excess charge trapped). From $\mathbf{A_{E\text{-}H}}$, the hole-trapped

dx.doi.org/10.1021/cs5010568 | ACS Catal. 2014, 4, 4051−4056

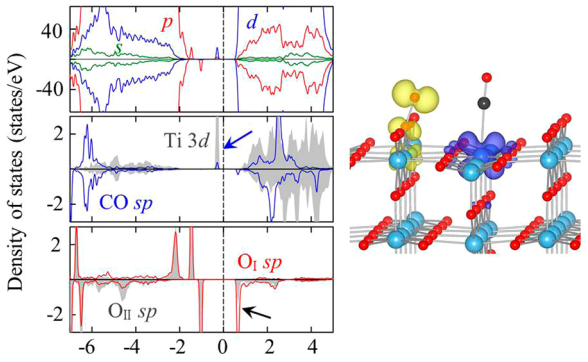

Figure 6. Density of states (DOS) for the electron−hole separated case of the partially reduced TiO_2(110) system with coadsorbed CO and O_2; the corresponding atomic configuration is shown on the right. The top, middle, and bottom panels respectively show the *s*, *p*, and *d* states of all C, O, and Ti atoms in the TiO_2(110) slab with CO and O_2, the 3*d* states of CO-bound Ti_{5c} and the CO *s* and *p* states, and the *s* and *p* states of O_2 (or O) at the O vacancy site, as indicated. In the structure illustration, the blue and yellow isosurfaces represent the localized excess electron (on Ti) and hole (on O_2) states as indicated by the arrows in the corresponding DOS plots. The isosurface value is set to 0.04 e/Å^3, and light blue, red, and dark gray balls represent Ti, O, and C atoms, respectively.

O_2 is found to lean preferentially toward the C (from CO) site (**B2**), rather than the Ti_{5c} site (**B1**). As shown in Figure 7, the energy barrier for the $\mathbf{A_{E\text{-}H}}$ (triplet) → **B2** (singlet) reaction is predicted to be 0.14 eV. In the calculations, we gradually changed the *x* coordinate of O_I toward C while fixing the *y* coordinates of O_I and C; the rest of the slab atoms were fully relaxed. This result clearly demonstrates that $\mathbf{A_{E\text{-}H}}$ can undergo reconfiguration to **B2** with no significant barrier. Once, the neutral intermediate (**B2**) is formed, CO_2 can desorb off the surface with a barrier of 0.32 eV (as explained earlier in Figure 2).

If another *h* could be added to the intermediate state, CO_2 desorption ($\mathbf{B_H}$ → $\mathbf{C_H}$) would likely take place with a lower barrier of 0.15 eV (as shown in Figure 4) (it would be also worth pointing out that, in the neutral intermediate state, an excess *e* prefers to localize on a subsurface Ti site, rather than the O−O—C−O complex, and thus has no impact on the **B** → **C** reaction, according to our calculations). Although an additional *h* appears to be important to further reduce the barrier for CO_2 desorption, the *h* remains at the bridging O site after desorption; hence, the net charge consumption turns out to be one *e* and one *h*, which is also consistent with recent experimental observations.[15] Our study clearly highlights the crucial role played synergistically by *e* and *h* in enabling facile CO oxidation by lowering the overall activation energy barrier (particularly at low temperatures where the thermal oxidation process may hardly occur because of the relatively high activation barriers required to overcome, as presented in Figure 2).

IV. SUMMARY

Using DFT calculations, we have investigated the contribution of photogenerated electrons and holes to the oxidation of CO on reduced TiO_2(110). For comparison, we first revisited thermally activated CO_2 production from coadsorbed CO and O_2, which confirms two possible pathways each of which involves an intermediate state forming an either O−O−Ti—C−O or O−O−C−O complex; the overall energy barriers are predicted to be about 0.78 and 0.87 eV, respectively. When an excess *h* is present, the O_2 that initially resides horizontally at the O vacancy site adopts a tilted open ring configuration, which allows the O−O−C−O complex formation by overcoming an activation energy of 0.49 eV. In the intermediate state, the CO binding is found to be weakened due to largely delocalized *h* charge over the O−O−C−O complex, which in turn facilitates CO_2 production with a relatively low energy barrier of 0.15 eV. However, the predicted barrier of 0.49 eV for the first-step reaction appears to be still too high for facile CO oxidation at low temperatures. On the other hand, our DFT calculations demonstrate that the barrier for the O_2 + CO → O−O−C−O reaction can be significantly reduced by the presence of excess *e* and *h* (which tends to localize on the CO-bound Ti atom and the terminal O atom in the open ring O_2, respectively); the separate *e* and *h* configuration in the triplet state is predicted to undergo reconfiguration to the intermediate O−O−C−O singlet state with a small barrier of 0.14 eV. From the neutral intermediate state, CO_2 can desorb off the surface with a barrier of about 0.3 eV (or a lower barrier of 0.15 eV if another *h* is supplied). Our study clearly highlights the synergetic contribution of photogenerated *e* and *h* to facile CO oxidation. This also provides unequivocal theoretical support for a recent experimental study suggesting involvement of multiple nonthermal reaction steps in low-temperature CO photooxidation.

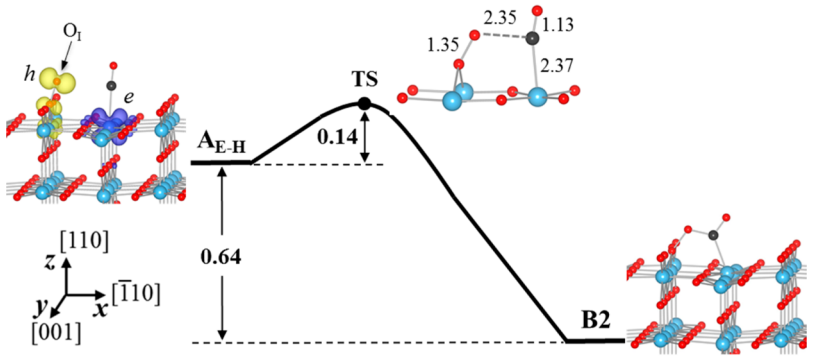

Figure 7. Predicted potential energy variation (in eV) along the minimum energy pathway for reconfiguration of the *e*-*h* separated triplet state ($\mathbf{A_{E\text{-}H}}$) to the singlet O−O−C−O complex (**B2**), together with the $\mathbf{A_{E\text{-}H}}$, **B2** and transition state (**TS**) configurations; selected bond distances are also shown in Å, and light blue, red, and dark gray balls represent Ti, O, and C atoms, respectively. In the $\mathbf{A_{E\text{-}H}}$ structure, the blue and yellow isosurfaces (corresponding to 0.04 e/Å^3) represent the localized excess electron (on Ti) and hole (on O_2) states.

dx.doi.org/10.1021/cs5010568 | *ACS Catal.* 2014, 4, 4051−4056

■ ASSOCIATED CONTENT

Supporting Information

Table S1 and Figures S1−S3. This material is available free of charge via the Internet at http://pubs.acs.org.

■ AUTHOR INFORMATION

Corresponding Author

*E-mail: gshwang@che.utexas.edu.

Notes

The authors declare no competing financial interest.

■ ACKNOWLEDGMENTS

This work was supported by the Korea CCS R&D Center (KCRC) grant (No. 2014049270) funded by the Korea government (Ministry of Science, ICT & Future Planning), the R. A. Welch Foundation (No. F-1535), and the National Science Foundation (DMR-1122603). We would like to thank the Texas Advanced Computing Center for use of their computing resources.

■ REFERENCES

(1) Linsebigler, A. L.; Lu, G.; Yates, J. T. *Chem. Rev.* **1995**, *95*, 735−758.
(2) Hashimoto, K.; Irie, H.; Fujishima, A. *Jpn. J. Appl. Phys.* **2005**, *44*, 8269−8285.
(3) Ni, M.; Leung, M. K. H.; Leung, D. Y. C.; Sumathy, K. *Renewable Sustainable Energy Rev.* **2007**, *11*, 401−425.
(4) Fujishima, A.; Zhang, X. T.; Tryk, D. A. *Surf. Sci. Rep.* **2008**, *63*, 515−582.
(5) Henderson, M. A. *Surf. Sci. Rep.* **2011**, *66*, 185−297.
(6) Sun, L.; Qin, Y.; Cao, Q.; Hu, B.; Huang, Z.; Ye, L.; Tang, X. *Chem. Commun.* **2011**, *47*, 12628−12630.
(7) Guan, K. *Surf. Coat. Technol.* **2005**, *191*, 155−160.
(8) Pillay, D.; Hwang, G. S. *J. Chem. Phys.* **2006**, *125*, 144706-1−144706-6.
(9) Ji, Y.; Wang, B.; Luo, Y. *J. Phys. Chem. C* **2013**, *117*, 956−961.
(10) Petrik, N. G.; Kimmel, G. A. *J. Phys. Chem. Lett.* **2010**, *1*, 2508−2513.
(11) Linsebigler, A.; Lu, G.; Yates, J. T. *J. Phys. Chem.* **1996**, *100*, 6631−6636.
(12) Lu, G.; Linsebigler, A.; Yates, J. T. *J. Chem. Phys.* **1995**, *102*, 3005−3008.
(13) Zhang, Z.; Yates, J. T. *J. Am. Chem. Soc.* **2010**, *132*, 12804−12807.
(14) Petrik, N. G.; Kimmel, G. A. *J. Phys. Chem. C* **2011**, *115*, 152−164.
(15) Petrik, N. G.; Kimmel, G. A. *J. Phys. Chem. Lett.* **2013**, *4*, 344−349.
(16) Dudarev, S. L.; Botton, G. A.; Savrasov, S. Y.; Humphreys, C. J.; Sutton, A. P. *Phys. Rev. B* **1998**, *57*, 1505−1509.
(17) Perdew, J. P.; Burke, K.; Ernzerhof, M. *Phys. Rev. Lett.* **1996**, *77*, 3865−3868.
(18) Kresse, G.; Furthmuller, J. *VASP: The Guide*; Vienna University of Technology: Vienna, 2001.
(19) Blöchl, P. E. *Phys. Rev. B* **1994**, *50*, 17953−17979.
(20) Deskins, N. A.; Rousseau, R.; Dupuis, M. *J. Phys. Chem. C* **2009**, *113*, 14583−14586.
(21) Deskins, N. A.; Rousseau, R.; Dupuis, M. *J. Phys. Chem. C* **2011**, *115*, 7562−7572.
(22) Deskins, N. A.; Dupuis, M. *J. Phys. Chem. C* **2009**, *113*, 346−358.
(23) Chrétien, S.; Metiu, H. *J. Phys. Chem. C* **2011**, *115*, 4696−4705.
(24) Muhich, C. L.; Zhou, Y.; Holder, A. M.; Weimer, A. W.; Musgrave, C. B. *J. Phys. Chem. C* **2012**, *116*, 10138−10149.
(25) Henrich, V. E.; Dresselhaus, G.; Zeiger, H. J. *Phys. Rev. Lett.* **1976**, *36*, 1335−1339.
(26) Yim, C. M.; Pang, C. L.; Thornton, G. *Phys. Rev. Lett.* **2010**, *104*, 036806-1−036806-4.
(27) Ji, Y.; Wang, B.; Luo, Y. *J. Phys. Chem. C* **2012**, *116*, 7863−7866.
(28) Shibuya, T.; Yasuoka, K.; Mirbt, S.; Sanyal, B. *J. Phys.: Condens. Matter* **2012**, *24*, 435504-1−435504-8.
(29) Janotti, A.; Varley, J. B.; Rinke, P.; Umezawa, N.; Kresse, G.; Van de Walle, C. G. *Phys. Rev. B* **2010**, *81*, 085212-1−085212-7.
(30) Kweon, K. E.; Hwang, G. S. *Phys. Rev. B* **2013**, *87*, 205202-1−205202-6.
(31) Henkelman, G.; Uberuaga, B. P.; Jónsson, H. *J. Chem. Phys.* **2000**, *113*, 9901−9904.
(32) Henkelman, G.; Jónsson, H. *J. Chem. Phys.* **1999**, *111*, 7010−7022.
(33) Pacchioni, G.; Ferrari, A. M.; Bagus, P. S. *Surf. Sci.* **1996**, *350*, 159−175.
(34) Sorescu, D. C.; Yates, J. T. *J. Phys. Chem. B* **1998**, *102*, 4556−4565.
(35) Yang, Z.; Wu, R.; Zhang, Q.; Goodman, D. W. *Phys. Rev. B* **2001**, *63*, 045419-1−045419-6.
(36) Menetrey, M.; Markovits, A.; Minot, C. *Surf. Sci.* **2003**, *524*, 49−62.
(37) Wang, Y.; Pillay, D.; Hwang, G. S. *Phys. Rev. B* **2004**, *70*, 193410-1−193410-4.
(38) Rohmann, C.; Wang, Y.; Muhler, M.; Metson, J.; Idriss, H.; Wöll, C. *Chem. Phys. Lett.* **2008**, *460*, 10−12.
(39) Cococcioni, M.; de Gironcoli, S. *Phys. Rev. B* **2005**, *71*, 035105-1−035105-16.
(40) Cohen, J.; Mori-Sanchez, P.; Yang, W. *Science* **2008**, *321*, 792−794.
(41) Sung, S. S.; Hoffmann, R. *J. Am. Chem. Soc.* **1985**, *107*, 578−584.
(42) Gajdoš, M.; Eichler, A.; Hafner, J. *J. Phys.: Condens. Matter* **2004**, *16*, 1141−1164.